Impedance Analysis of Piezoelectric Energy Harvesting System Using Synchronized Charge Extraction Interface Circuit

Chen Chen, Kang Zhao, and Junrui Liang

School of Information Science and Technology, ShanghaiTech University
No. 393, Middle Huaxia Road, Pudong, Shanghai 201210, China

ABSTRACT

The synchronous charge extraction (SCE) interface circuit is unique among the existing piezoelectric energy harvesting (PEH) power conditioning circuits, for its output power is independent of the load. The previous studies about SCE have assumed lossless rectifier and ideal energy transfer through the inductor; the detailed energy flow picture in SCE was absent. This paper provides an impedance based analysis for the PEH system using SCE interface circuit. Through qualitative analysis on the energy cycle, the electrically induced dynamics of SCE is broken down into three components: the accompanied capacitance, dissipative resistance, and harvesting resistance, which correspond to an additional stiffness, a dissipative damper, and a regenerative damper, respectively, to the mechanical structure. Quantitative analysis on the harvested power is also carried out. Experiments on practical PEH system show good agreement with the theoretical results. The new insight provided in this study help better understand the dynamics and better evaluate the harvesting capability of the SCE circuit among those options of power conditioning towards practical PEH implementations.

Keywords: Piezoelectric energy harvesting, impedance analysis, synchronized charge extraction

1. INTRODUCTION

The energy harvesting technologies provide the possibility to convert the ambient energy from different physical sources, e.g., solar, thermal, wind, vibration, into useful electricity. Wireless sensor networks (WSNs) and mobile electronics are two of the most potential applications pushing forward the development of these technologies.[1] For energy harvesting from ambient vibration sources, it has been shown that the improvement of power conditioning circuit design makes a big contribution towards the harvesting capability enhancement.[2] In particular, the power conditioning circuits of piezoelectric energy harvesting (PEH) systems have received much research attention during the last decade.[3–6]

The most convenient way to realize the ac-to-dc power conversion is to utilize a full-wave bridge rectifier.[3] It is fully passive and easy to be implemented. Therefore, the full-wave bridge rectifier is usually referred to as the standard energy harvesting (SEH) interface circuit for PEH. Besides the passive bridge rectifier, some semi-passive solutions were extensively studied. The most investigated circuits in the semi-passive family are called synchronized switch harvesting on inductor (SSHI).[7,8] By taking the synchronized switch actions, the harvested power can be increased by several folds. More recently, there are some solutions utilizing the semi-active approach to further enhance the harvesting capability beyond SSHI. For instance, the single supply pre-biasing (SSPB)[9] and the parallel synchronized triple bias-flip (P-S3BF).[5,10]

The harvested power in all the aforementioned power conditioning circuits are load depended. In other words, without additional maximum power point tracking (MPPT) module, the enhancement on harvested power can not be guaranteed under load variation. There is one exceptional circuit, which realizes the load independent feature. It is called the synchronous charge extraction (SCE).[11] Since the harvested power does not change with load variation, no addtional MPPT effort is needed. Given its merit of load independence, the SCE, even its peak performance is not the best, has received much attention from the practical point of view.

Corresponding author: Junrui Liang. E-mail: liangjr@shanghaitech.edu.cn.

Active and Passive Smart Structures and Integrated Systems 2017, edited by
Gyuhae Park, Alper Erturk, Jae-Hung Han, Proc. of SPIE Vol. 10164, 101642Q
 · doi: 10.1117/12.2261095

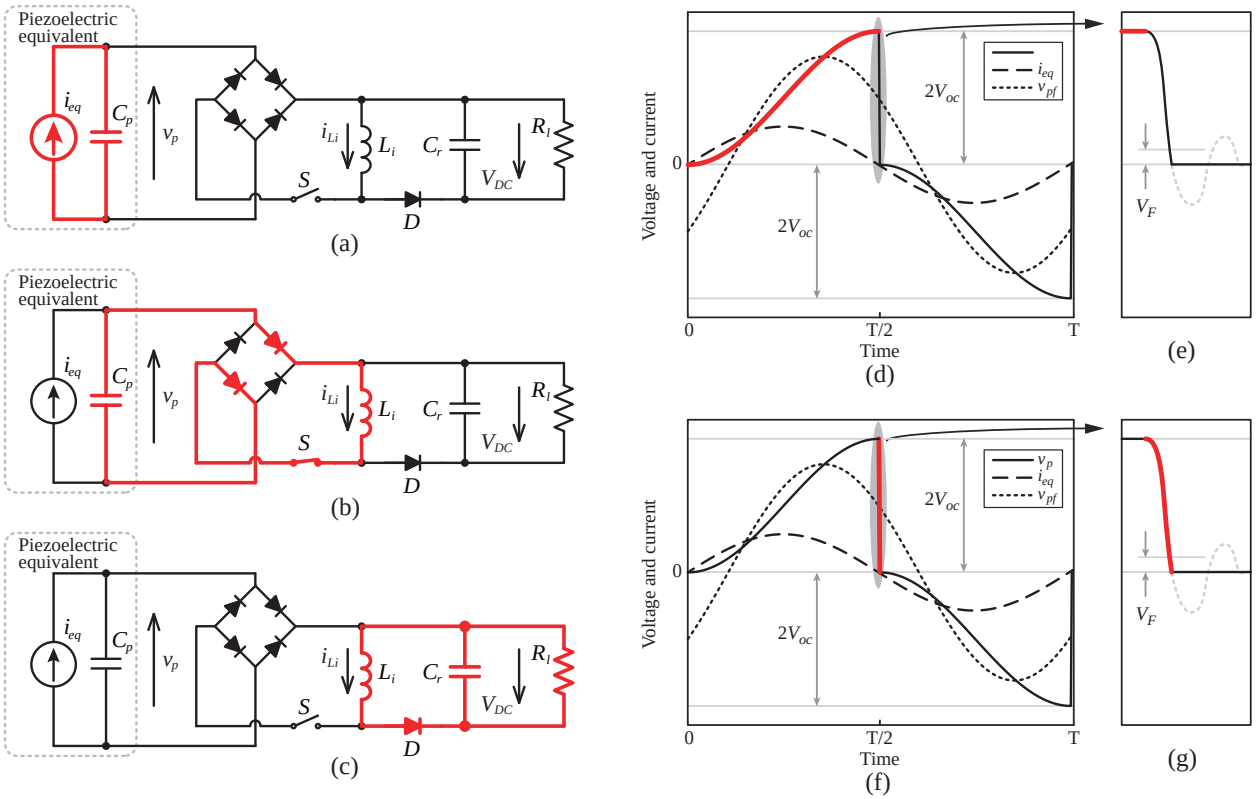

Figure 1. Operating phases and waveforms in SCE interface circuit. (a) Open-circuited phase. (b) Switch phase at displacement extremes. (c) Freewheeling charge phase. (d) Voltage and current at the open-circuit phase. (e) Enlarged view of the switching instant. (f) Voltage and current at the switch phase. (g) Enlarged view of the switching instant.

A practical PEH system is the synergy of a mechanical vibrator, piezoelectric transducer, and power conditioning circuit. A joint dynamic model of the entire system is important towards precise prediction on harvested power. For the power analysis of SEH and SSHI, in-phase model was used at the beginning.[7] It is only valid at resonance. Shu et al. later proposed an improved analysis, which covers both the resonance and off-resonance dynamics.[12,13] Liang and Liao refined the energy flow concept[14] and proposed an equivalent impedance model. In their model, the circuit dynamics is disassembled into three detailed components; therefore, it provides a more in-depth understanding on the effects of practical power conditioning circuits.[15]

For the analysis of SCE, early studies were also based on the in-phase principle, which focuses on the resonance.[11] The improved analysis, which covers the whole frequency span was transplanted to SCE later by Tang and Yang.[16] Yet, the impedance based analysis is absent up to now. On the other hand, in the previous analyses, ideal lossless rectifier and lossless switch action were assumed in the analysis. The ratio between harvested power and dissipated power within the power conditioning process was not fully revealed. This paper provides an impedance analysis for the PEH system using SCE interface circuits, and at the same time, takes the possible power dissipation during the power conditioning process into consideration, in order to fill the gap of theoretical analysis of SCE interface circuit.

2. OPERATING PRINCIPLE

Figure 1 illustrates the working principle of SCE by showing the conducting circuit branches and waveforms of different phases in half of an operating cycle. In the figure, the piezoelectric element is modeled as a current source i_{eq}, whose value is proportional to the vibration velocity, in parallel with its clamped capacitance C_p. From the power electronics point of view, the SCE circuit is composed of a full-wave rectifier bridge and a buck-boost circuit as illustrated in Figure 1(a)–(c).

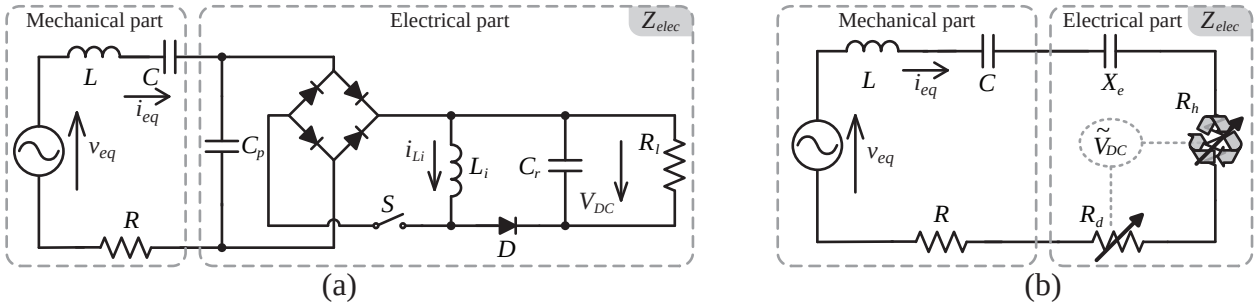

Figure 2. (a) Equivalent circuit. (b) Equivalent impedance network.

In SCE, each half cycle can be divided into three phases: the open-circuit phase, switch phase, and freewheeling charge phase. In the open-circuit phase shown in Figure 1(a), the SCE circuit makes no intervention to the piezoelectric structure; therefore, C_p is freely charged by the equivalent current source i_{eq} from the initial voltage of zero. The second phase takes place when i_{eq} crosses zero, i.e., the vibration displacement is maximized, since i_{eq} is proportional to the vibration velocity. The synchronized switch S turns on and enables the charge stored in C_p to flow through the intermediary inductor L_i, the potential energy is converted into kinetic one in L_i. This phase will automatically end (suppost the switch-on duration is longer than one fourth of the L_iC_p cycle) when v_p the voltage across the piezoelectric element drops to zero, since v_p is also the input of the bridge rectifier. A bridge rectifier conducts only when the product of the input current and the voltage difference between input and output voltages is positive. In other words, it only absorbs power from the input. After the switch phase, the energy that is trapped in L_i has no way to go but only go through the diode D and the filter capacitor C_r and load resistor R_l. This is the third freewheeling charge phase. In the $i_{eq} < 0$ half cycle, there are other three similar phases, whose working principles are not repeated here.

As we can observed from Figure 1, the synchronized switch actions make v_p and i_{eq} always have the same sign, i.e., both are positive or negative. The amount of charge removal in each switch action is the same as well, given that the magnitude and frequency of i_{eq} do not change. Such constant charge removal enables the unique feature of SCE on load independence.

Previous literature assume ideal rectification and freely charge movement in analysis. Yet, for practical circuits, energy dissipation is unavoidable in the power conditioning process. Based on the framework of energy flow and equivalent impedance analysis,[14,15] the dissipated power also has an effect over the system dynamics. With a scrutiny to the SCE circuit, we can find that, there are three possible ways causing energy dissipation: the practical bridge rectifier with forward voltage drop V_F, the non-ideal energy transfer from C_p to L_i, given a finite quality factor Q, the practical freewheeling diode D with forwards voltage drop V_D. A more accurate model for practical SCE circuit should also take these details into consideration.

3. DYNAMICS OF THE MECHANICAL PART

For studying the joint dynamics of the SCE solution for PEH, we should also incorporate with the mechanical dynamics in the model. As the current source equivalent shown in Figure 1 has oversimplified the resonant feature of the mechanical structure. We use an additional series RLC circuit to model the first-mode vibration of the structure. The more complete equivalent circuit is shown in Figure 2(a). Those components R, L, C, and v_{eq} come from electromechanical analogy, which corresponds to the damping D, mass M, stiffness K, and force source $f(t)$ with the relations as follows[15]

$$R = \frac{D}{\alpha_e^2}, \qquad C = \frac{\alpha_e^2}{K}, \qquad L = \frac{M}{\alpha_e^2}, \tag{1}$$

$$v_{eq}(t) = \frac{f(t)}{\alpha_e}, \qquad i_{eq}(t) = \alpha_e \dot{x}(t), \tag{2}$$

where α_e is the force-voltage factor.

Given the nonlinear nature of a bridge rectifier, its equivalent impedance is unable to be formulated without considering the source impedance of the piezoelectric source. Therefore, in the impedance based analysis, the overall dynamic effect of the source impedance sC_p (s is the Laplace variable) and the connected circuit is usually considered together and taken as Z_{elec} the equivalent impedance of the electrical part here, as shown in Figure 2(a). With this designation, the equivalent circuit shown in Figure 2(a) can be mathematically formulated as follows

$$\frac{V_{eq}(s)}{I_{eq}(s)} = \left[R + \frac{1}{sC} + sL + Z_{elec}(s)\right]. \tag{3}$$

4. IMPEDANCE OF THE ELECTRICAL PART

In Figure 2, the entire PEH system is classified into mechanical and electrical parts. The key problem working towards the joint dynamic model, in terms of equivalent impedance, is how to properly formulate the dynamics of Z_{elec} approximating to the actual dynamics of the bridge rectifier and C_p combination.

In the impedance modeling for SEH and SSHI circuits, we start from assuming the harmonic current $i_{eq}(t)$ as follows

$$i_{eq}(t) = \alpha_e \omega X \sin(\omega t) = I_0 \sin(\omega t), \tag{4}$$

where X is displacement magnitude of the mechanical vibrator. Such assumption makes sense given that the mechanical inertia smooths the vibrating movement, such that the velocity $\dot{x}(t)$ can maintain sinusoidal without large backward electrically induced force.

Based on the harmonic current assumption, the voltage across the piezoelectric element $v_p(t)$ can be formulated as a piecewise function given the initial conditions and charge relations in different phases as illustrated in Figure 1. The v_p expression can be obtained as follow

$$v_p(t) = V_{oc} \times \begin{cases} 1 - \cos(\omega t), & 2k\pi \le \omega t < (2k+1)\pi, \\ -1 - \cos(\omega t), & (2k+1)\pi \le \omega t < 2(k+1)\pi, \end{cases} \tag{5}$$

where

$$V_{oc} = \frac{I_0}{\omega C_p} = \frac{\alpha_e X}{C_p} \tag{6}$$

is the magnitude of the open circuit voltage. Based on (6), the fundamental harmonic of $v_p(t)$ therefore can be expressed as follows

$$v_{pf}(t) = -V_{oc}\cos(\omega t) + \frac{4V_{oc}}{\pi}\sin(\omega t). \tag{7}$$

The curve of $v_{pf}(t)$ is also plotted in Figure 1(d) and (f).

With the sinusoidal current and voltage formulated in (4) and (7), the dynamics of Z_{elec} therefore can be linearly approximated by the ratio of V_{pf} over I_{eq}, as follows

$$Z_{elec}(s) = \frac{V_{pf}(s)}{i_{eq}(s)} = \frac{1}{\omega C_p}\left(\frac{4}{\pi} - j\right). \tag{8}$$

It can be observed from (8) that Z_{elec} is a constant complex number, whose imaginary part is equal to the impedance of the open-circuit situation, i.e., $(sC_p)^{-1}$. In other words, no matter how the electrical load changes, the electrically induced dynamics by SCE is identical.

The equivalent impedance Z_{elec} of PEH systems with other three commonly discussed interface circuits (SEH, P-SSHI, and S-SSHI) have been derived and comparatively studied.[17] In those cases, their equivalent impedance varies along with different specified trajectories by changing the rectified voltage, rather than can be arbitrarily assigned in the complex plane. Given the degree of freedom for the variation of equivalent impedance, optimal impedance point, which gives maximum harvested power, exist for either of these solutions. However, for SCE, there is no way to adjust the joint dynamics, because its equivalent impedance is a constant. The equivalent impedance Z_{elec} in SEH, SSHI, and SCE are illustrated in Figure 3.

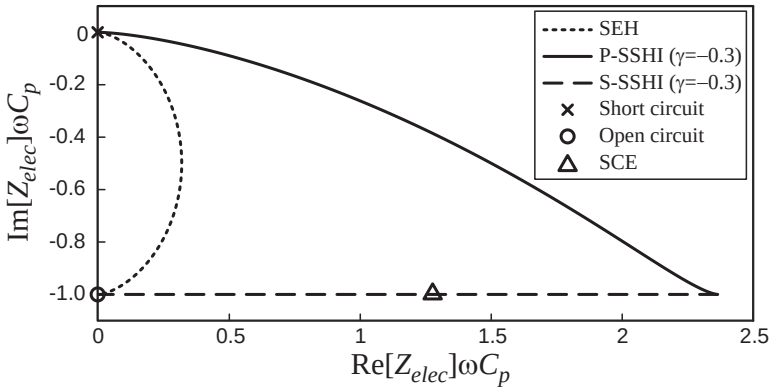

Figure 3. Electrical part equivalent impedance with four different interface circuits.

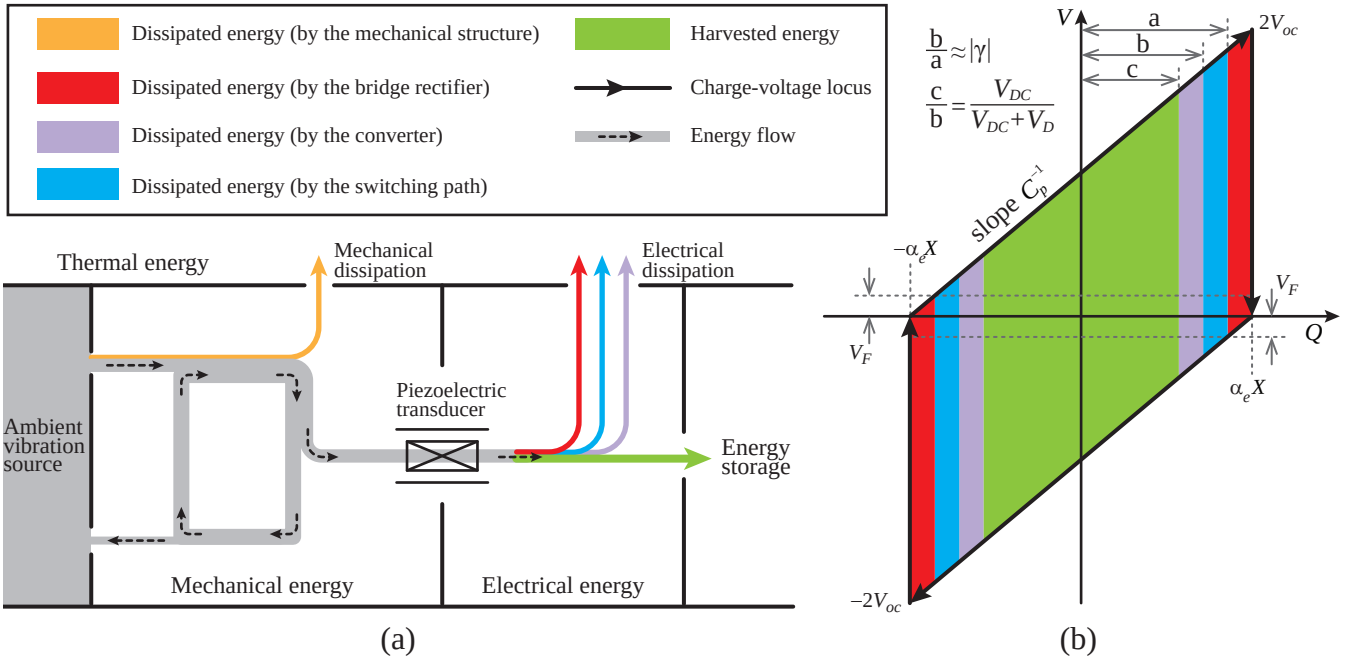

Figure 4. Analysis on the detailed energy composition in SCE. (a) Energy flow chart. (b) The energy cycle.

The real part of Z_{elec} is related to the power extracting capability from the piezoelectric structure. In weakly coupled condition, the magnitude of source impedance, even in resonance, is much larger than that of Z_{elec}. Under this situation, the extracted power is just proportional to the real part of Z_{elec}. Therefore, SCE has better performance than SEH but less capable than SSHI, in terms of energy removal capability from the vibrating system, as we can observe by comparing their real parts in Figure 3.

5. ENERGY FLOW

Z_{elec} just represents the overall dynamics of the C_p and harvesting circuit combination. The real part of Z_{elec} relates to the energy extraction. In addition, since the extracted power might not be fully harvested into usefully energy, dissipation is unavoidable in the conditioning power electronics. Understanding the energy flow within the power conditioning circuit is important towards an accurate evaluation on our target, the harvested power.

The energy flow chart shown in Figure 4(a) gives intuition about the flowing directions of the energy in the PEH system using SCE circuit. The energy from the ambient vibration source enters the PEH system in a mechanical form. During vibration, some of the energy is dissipated, i.e., transformed into heat, through the

inherent mechanical damping. The mechanical dissipation is shown as the yellow branch in Figure 4(a). The gray ring in the mechanical domain represents the reactive power cycling between potential and kinetic energy in each vibration cycle. Piezoelectric transducer transforms a part of the mechanical energy into electrical one and extracts them from the mechanical part. As observed from Figure 4(a), the extracted energy has two destinations: one is converted into heat, i.e., dissipated; while the other is converted into electrical energy storage, i.e., harvested. The harvested energy is indicated by the green arrow in Figure 4(a). It is the targeted energy for PEH optimization. The energy dissipation are composed of three parts:

- energy dissipation caused by the non-ideal rectifier, denoted by red arrow;
- energy dissipation caused by the non-ideal switching RLC circuit, denoted by blue arrow;
- energy dissipation caused by the non-ideal freewheeling diode in the converter, denoted by purple arrow.

By clarifying the detailed energy dissipation in power conditioning, it shows again the conclusion in the previous impedance based analysis that the extracted power does not equal to the harvested power. Understanding their difference help better evaluate the harvesting capabilities of different interface circuits. Optimization should be done by not only increasing the extracted power, but at the same time, reducing the dissipated portion in the total power extraction.

Based on the qualitative understanding attained from the energy flow analysis, the amount of energy components can be further quantified. During each switch action in SCE, the piezoelectric voltage v_p immediately changes from V_{oc} or $-V_{oc}$ to zero as illustrated in Figure 1(d)–(g). The energy difference before and after the action is regarded as the energy extracted from the system in a half cycle. Therefore, the extracted energy in a half cycle is a constant

$$\Delta E = 2C_p V_{oc}^2. \tag{9}$$

During a switch action, the energy dissipated in the bridge rectifier, due to the forward voltage drop V_F, is

$$E_{d,bridge} = 2C_p V_{oc} V_F. \tag{10}$$

The amount of remaining energy is divided into two parts. One part is dissipated in the non-ideal $L_i C_p$ switching path, i.e.,

$$E_{d,switch} = 2(1+\gamma)C_p V_{oc}(V_{oc} - V_F), \tag{11}$$

where γ is related to the quality factor Q of the switching C_p-L_i-r path (r is the parasitic resistance in the path). γ is referred to as the inversion factor in the studies of SSHI,[7, 15] which is defined as follows

$$\gamma = -e^{-\pi/(2Q)}. \tag{12}$$

Even the voltage v_p in SCE is not "inverted", as that in the SSHI case, this factor still matters as the switch action in SCE is sort of the former half of that in SSHI. The rest part of the remaining energy is transfered into the intermediary inductor L_i, i.e.,

$$E_{Li,max} = 2|\gamma| C_p V_{oc}(V_{oc} - V_F), \tag{13}$$

The current through the inductor L_i at this moment is maximized and denoted as $I_{Li,max}$, as shown in Figure 5. After that, L_i charges the storage capacitor C_r through the freewheeling diode D. As the voltages across C_r and D are dc voltages, i_{Li} decreases with a constant slope $-(V_{DC} + V_D)$ as shown in Figure 5. Since the current flowing through C_r and D is the same, their energy absorptions are just proportional to their dc voltages. Therefore, the energy dissipated by D in the freewheeling charge phase can be obtained as follows

$$E_{d,converter} = \frac{V_D}{V_{DC} + V_D} E_{Li,max}. \tag{14}$$

And finally the harvested energy in a half cycle is obtained as follows

$$E_h = \frac{V_{DC}}{V_{DC} + V_D} E_{Li,max}. \tag{15}$$

The relation among those three dissipated portions and harvested portions in each cycle can be intuitively shown in the partitioned charge-force graph, which is also called the energy cycle of the PEH system, as shown in Figure 4(b).

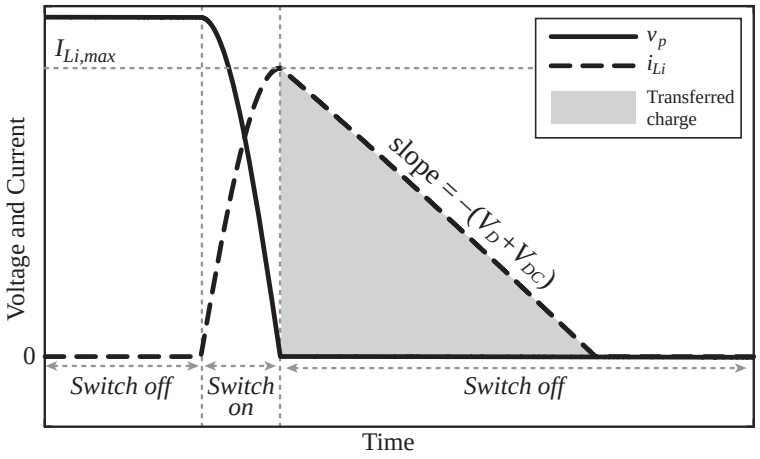

Figure 5. Enlarged view of v_p and i_{Li} in a synchronized switch instant of SCE.

6. DETAILED COMPONENTS AND EQUIVALENT IMPEDANCE NETWORK

Z_{elec} can be further broken down into three detailed components by quantifying the dynamic effects according to different energy flow branches. As the previous impedance modeling did, Z_{elec} can be divided into three components connected in series, i.e., the vibratory component X_e, harvesting component R_h, and dissipative component R_d. The energy absorbed by R_h corresponds to the harvested energy E_h in (15), the energy absorbed by R_d correspond to the sum of the three dissipated portions in (10), (11), and (14). The expressions of these three components are provided as follows

$$X_e = -\frac{1}{\omega C_p}, \tag{16}$$

$$R_h = \frac{4}{\pi\omega C_p}\frac{|\gamma|V_{DC}}{V_{DC}+V_D}\left(1-\tilde{V}_F\right), \tag{17}$$

$$R_d = \frac{4}{\pi\omega C_p}\left[\tilde{V}_F + \left(1+\frac{\gamma V_{DC}}{V_{DC}+V_D}\right)\left(1-\tilde{V}_F\right)\right]. \tag{18}$$

where $\tilde{V}_F = V_F/V_{oc}$ is the normalized forward voltage drop of the rectifier.

Figure 2(b) shows the equivalent impedance network of a PEH system using SCE, in which all the mechanical and electrical dynamics are expressed in a same "language". The symbols of R_h and R_d are marked with arrows to indicate that their values are variables as functions of the normalized output dc voltage $\tilde{V}_{DC} = V_{DC}/V_{oc}$. On the other hand, since the imaginary part of Z_{elec} in SCE case is a constant, it is not affected by $\tilde{V}_{DC}$. Such equivalent impedance network model can be utilized to quantify the harvested power under constant force magnitude excitation as follows

$$P_h = \frac{V_{eq}^2}{2}\frac{R_h}{\left(X_L+X_C+X_e\right)^2+\left(R+R_d+R_h\right)^2}. \tag{19}$$

According to (19), the harvested power is a function of the vibration frequency and the normalized output dc voltage $\tilde{V}_{DC} = V_{DC}/V_{oc}$. Therefore, detailed scrutiny finds that, unlike what was strongly claimed by the previous literature, the harvested power P_h in fact is weakly depended on the loading condition, which has an effect over the dc output voltage V_{DC}.

7. EXPERIMENTS

Experiments are carried out on a base excited PEH system. The experimental setup is shown in Figure 6. A piezoelectric bimorph is fixed at the base structure, which is excited by a shaker. A pair of magnets are attached at the free end of the piezoelectric cantilever. With the coaxial coils installed at the base structure, the magnet

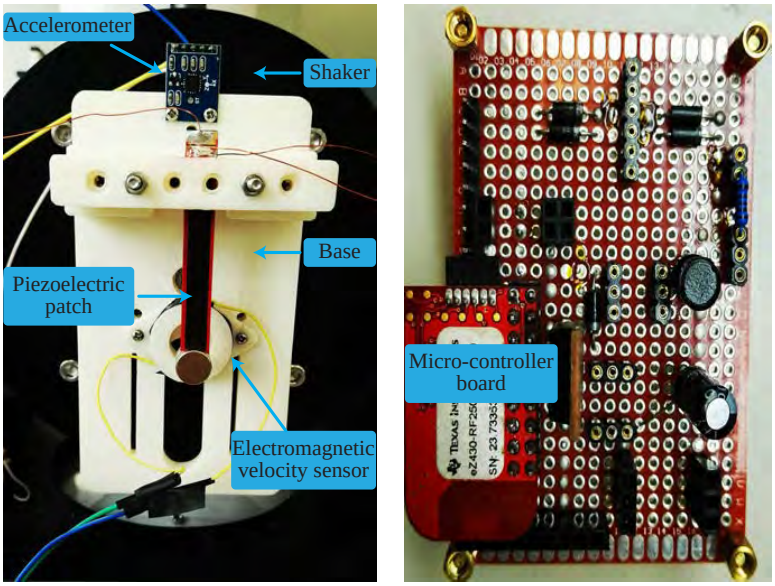

Figure 6. Experimental setup. (a) The mechanical installation. (b) The prototyped SCE circuit.

and coil pairs form an electromagnetic sensor for velocity sensing. At the same time, the magnet pair also acts as a proof mass, which reduces the resonant frequency and increases the deflection magnitude. The output voltage of the coil is proportional to the relative speed of the cantilever deflection. The sensed signal is input to the MCU for providing synchronized switch control to a MOSFET switch. such that to operate the SCE circuit. An accelerometer is installed at the base for maintaining constant magnitude for the base acceleration, such that to make sure the excitation criteria. Figure 6(b) shows the prototyped SCE interface circuit. The bridge rectifier is built with four diodes. A current sensing resistor is connected in between the rectifier bridge output and the intermediary inductor for monitoring the current through the inductor. The specifications of the PEH systems are listed in Table 1.

In experiment, the SEH and SCE circuits are comparatively studied and validated, Their harvested power under different dc output voltage is recorded by connecting different load resistor R_l under constant base acceleration magnitude excitation. The experimental harvested power P_h is obtained as follows

$$P_{h,exp} = \frac{V_{DC}^2}{R_l}, \tag{20}$$

The experimental waveform of SCE is shown in Figure 7(a). It agrees with the expected waveform. The theoretical and experimental results on harvested power in SEH and SCE are shown in Figure 7(b). The theoretical prediction makes a good agreement with the experimental measurement under the specific excitation condition. More accurate evaluation on the harvested power is obtained based on the impedance based analysis. In particular, for the small V_{DC} region, experimental results in the previous literature all showed the exponential-shape changing trend; yet, there was no explanation about the reason. We manage to model this practical problem, which violates the load independence feature based on the impedance modeling. On the other hand, the reason why it seems that the SEH circuit outperforms the SCE, in terms of maximum harvested power, is because the strongly coupled feature of the experimental piezoelectric structure. Tang and Yang have pointed out that SEH will outperform SCE under strongly coupled condition.[16]

8. CONCLUSION

The equivalent impedance model provides an effective analytical methodology for studying the electromechanical joint dynamics of the piezoelectric energy harvesting (PEH) systems. This paper has extended its application

Table 1. Specifications of the experimental PEH system.

Parameter	Value	Parameter	Value
Base acceleration $\ddot{Y}$	7.0 m/s^2	R	71.68 kΩ
Open circuit voltage V_{oc}	21.4 V	L	2.70 kH
Rectifier	4 diodes (1N4004)	C	3.06 nF
Switch	MOSFET (IRL540N)	C_p	69.31 nF
V_D	1.0 V	α_e	2.1×10^{-3} N/V
V_F	2.0 V	γ	−0.35
C_r	10 μF	f_0	56 Hz
L_i	47 mH		

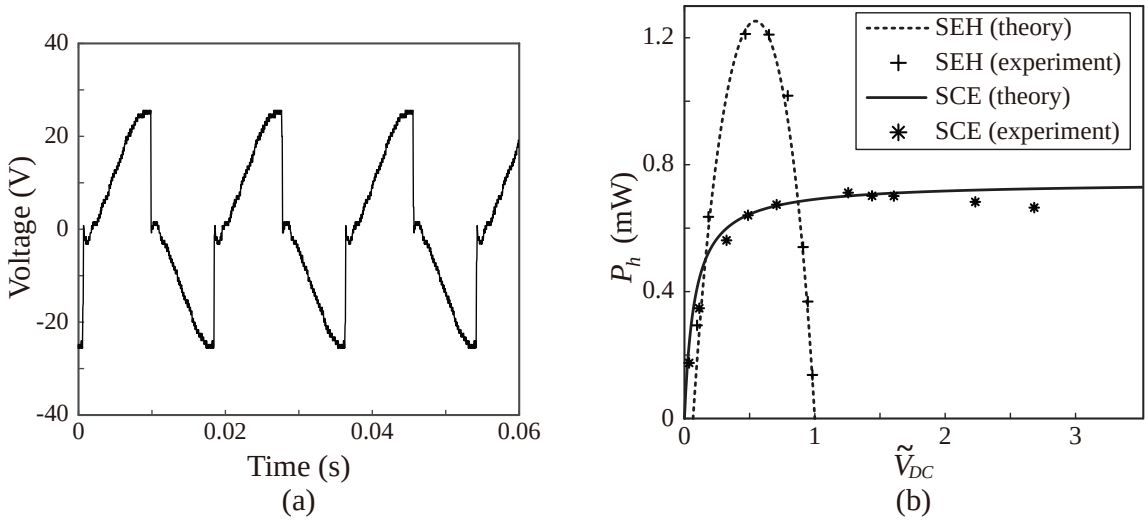

Figure 7. Experimental resutls. (a) Voltage waveform in experiment. (b) Theoretical and experimental results on harvested power.

to the analysis of PEH systems using SCE interface circuit. It helps better evaluate the energy dissipation in the power conditioning circuit, better understand the pros and cons of SCE under different operating conditions. Experimental results on harvested power have validated our analysis. It shows that, in practical SCE circuit, the harvested power is still weakly depended on the output dc voltage, rather than strictly constant along the whole span of different load resistance. Nevertheless, the harvested power is still relatively stable over different loading resistance, compared to other solutions. Therefore, SCE is still unique and capable for building compact and robust PEH systems.

ACKNOWLEDGMENTS

The work described in this paper was supported by the grants from National Natural Science Foundation of China (Project No. 61401277) and ShanghaiTech University (Project No. F-0203-13-003).

REFERENCES

[1] Paradiso, J. A. and Starner, T., "Energy scavenging for mobile and wireless electronics," *IEEE Pervasive Comput.* **4**(1), 18–27 (2005).

[2] Szarka, G. D., Stark, B. H., and Burrow, S. G., "Review of power conditioning for kinetic energy harvesting systems," *IEEE Trans. Power Electron.* **27**(2), 803–815 (2012).

[3] Ottman, G. K., Hofmann, H. F., and Lesieutre, G. A., "Optimized piezoelectric energy harvesting circuit using step-down converter in discontinuous conduction mode," *IEEE Trans. Power Electron.* **18**(2), 696–703 (2003).

[4] Badel, A., Benayad, A., Lefeuvre, E., Lebrun, L., Richard, C., and Guyomar, D., "Single crystals and nonlinear process for outstanding vibration-powered electrical generators," *IEEE Trans. Ultrason. Ferroelectr. Freq. Control* **53**(4), 673–684 (2006).

[5] Zhao, Y. and Liang, J., "Synchronized triple bias-flip circuit for piezoelectric energy harvesting enhancement: Operation principle and experimental validation," in [*Proceedings of the 2016 IEEE Energy Conversion Congress and Exposition (ECCE)*], 1–6 (2016).

[6] Liang, J., "Synchronized bias-flip interface circuits for piezoelectric energy harvesting enhancement: A general model and prospects," *J. Intell. Mater. Syst. Struct.* **28**(3), 339–356 (2017).

[7] Guyomar, D., Badel, A., Lefeuvre, E., and Richard, C., "Toward energy harvesting using active materials and conversion improvement by nonlinear processing," *IEEE Trans. Ultrason. Ferroelectr. Freq. Control* **52**(4), 584–595 (2005).

[8] Lefeuvre, E., Badel, A., Richard, C., Petit, L., and Guyomar, D., "A comparison between several vibration-powered piezoelectric generators for standalone systems," *Sens. Actuators, A* **126**(2), 405–416 (2006).

[9] Dicken, J., Mitcheson, P. D., Stoianov, I., and Yeatman, E. M., "Power-extraction circuits for piezoelectric energy harvesters in miniature and low-power applications," *IEEE Trans. Power Electron.* **27**(11), 4514–4529 (2012).

[10] Zhao, Y., Zhou, C., and Liang, J., "Implementation of synchronized triple bias-flip interface circuit towards higher piezoelectric energy harvesting capability," in [*Proceedings of the 26th International Conference on Adaptive Structures and Technologies*], ICAST (2015).

[11] Lefeuvre, E., "Piezoelectric energy harvesting device optimization by synchronous electric charge extraction," *J. Intell. Mater. Syst. Struct.* **16**(10), 865–876 (2005).

[12] Shu, Y. C. and Lien, I. C., "Analysis of power output for piezoelectric energy harvesting systems," *Smart Mater. Struct.* **15**(6), 1499–1512 (2006).

[13] Shu, Y. C., Lien, I. C., and Wu, W. J., "An improved analysis of the SSHI interface in piezoelectric energy harvesting," *Smart Mater. Struct.* **16**(6), 2253–2264 (2007).

[14] Liang, J. R. and Liao, W. H., "Energy flow in piezoelectric energy harvesting systems," *Smart Mater. Struct.* **20**(1), 015005 (2011).

[15] Liang, J. and Liao, W.-H., "Impedance modeling and analysis for piezoelectric energy harvesting systems," *IEEE/ASME Trans. Mechatron.* **17**(6), 1145–1157 (2012).

[16] Tang, L. and Yang, Y., "Analysis of synchronized charge extraction for piezoelectric energy harvesting," *Smart Mater. Struct.* **20**(8), 085022 (2011).

[17] Liang, J. and Liao, W.-H., "Piezoelectric energy harvesting and dissipation on structural damping," *J. Intell. Mater. Syst. Struct.* (2008).